The Role of the Indonesian Throughflow in the Indo–Pacific Climate Variability in the GFDL Coupled Climate Model

QIAN SONG
Program in Atmospheric and Oceanic Sciences, Princeton University, Princeton, New Jersey

GABRIEL A. VECCHI
UCAR Visiting Scientist, GFDL, Princeton, New Jersey

ANTHONY J. ROSATI
National Oceanic and Atmospheric Administration/Geophysical Fluid Dynamics Laboratory, Princeton, New Jersey

(Manuscript received 15 June 2006, in final form 7 September 2006)

ABSTRACT

The impacts of the Indonesian Throughflow (ITF) on the tropical Indo–Pacific climate, particularly on the character of interannual variability, are explored using a coupled general circulation model (CGCM). A pair of CGCM experiments—a control experiment with an open ITF and a perturbation experiment in which the ITF is artificially closed—is integrated for 200 model years, with the 1990 values of trace gases. The closure of the ITF results in changes to the mean oceanic and atmospheric conditions throughout the tropical Indo–Pacific domain as follows: surface temperatures in the eastern tropical Pacific (Indian) Ocean warm (cool), the near-equatorial Pacific (Indian) thermocline flattens (shoals), Indo–Pacific warm-pool precipitation shifts eastward, and there are relaxed trade winds over the tropical Pacific and anomalous surface easterlies over the equatorial Indian Ocean. The character of the oceanic changes is similar to that described by ocean-only model experiments, though the amplitude of many features in the tropical Indo–Pacific is amplified in the CGCM experiments.

In addition to the mean-state changes, the character of tropical Indo–Pacific interannual variability is substantially modified. Interannual variability in the equatorial Pacific and the eastern tropical Indian Ocean is substantially intensified by the closure of the ITF. In addition to becoming more energetic, El Niño–Southern Oscillation (ENSO) exhibits a shorter time scale of variability and becomes more skewed toward its warm phase (stronger and more frequent warm events). The structure of warm ENSO events changes; the anomalies of sea surface temperature (SST), precipitation, and surface westerly winds are shifted to the east and the meridional extent of surface westerly anomalies is larger.

In the eastern tropical Indian Ocean, the interannual SST variability off the coast of Java–Sumatra is noticeably amplified by the occurrence of much stronger cooling events. Closing the ITF shoals the eastern tropical Indian Ocean thermocline, which results in stronger cooling events through enhanced atmosphere–thermocline coupled feedbacks. Changes to the interannual variability caused by the ITF closure rectify into mean-state changes in tropical Indo–Pacific conditions. The modified Indo–Pacific interannual variability projects onto the mean-state differences between the ITF open and closed scenarios, rectifying into mean-state differences. These results suggest that CGCMs need to reasonably simulate the ITF in order to successfully represent not just the mean climate, but its variations as well.

1. Introduction

The Indonesian Throughflow (ITF) acts as an oceanic connection between the warm pools of the Pacific and Indian Oceans. Observations of the ITF show that in the mean it transports ~10 Sv (1 Sv $\equiv 10^6$ m^3 s^{-1}) of warm and fresh water from the tropical Pacific Ocean to the tropical Indian Ocean, and that it exhibits substantial variability on a variety of time scales (see Gordon 2001 for review). The ITF plays an integral role in the global thermohaline circulation, and has strong impacts on the mass, heat, and freshwater budgets for both the Indian and Pacific Oceans (Gordon 1986, 2001). The influence of the ITF on the climate remains an active research topic (Gordon 2005).

Corresponding author address: Dr. Qian Song, NOAA/Geophysical Fluid Dynamics Laboratory, P.O. Box 308, 201 Forrestal Rd., Princeton, NJ 08542.
E-mail: Qian.Song@noaa.gov

DOI: 10.1175/JCLI4133.1

Early theoretical studies (e.g., Clarke 1991; du Penhoat and Cane 1991; Spall and Pedlosky 2005) on the impacts of the ITF focused on the reflection efficiency of the equatorial Rossby waves at the leaky western Pacific boundary and its role in El Niño–Southern Oscillation (ENSO). Subsequently, the effects of the ITF on the large-scale ocean circulation were investigated with ocean-only models, by contrasting ITF-on and -off experiments (e.g., Hughes et al. 1992; Hirst and Godfrey 1993; Godfrey 1996; Murtugudde et al. 1998; Lee et al. 2002; Song and Gordon 2004). Although these studies could not fully address how the air–sea coupled climate system may be affected by ITF, they quantified the direct effects of the ITF within the oceans, and their results form a basis for further coupled model studies upon which to build. The key conclusion of these ocean-only model studies is that by carrying warm water from the western Pacific to the Indian Ocean, the ITF warms the upper Indian Ocean and deepens its thermocline, while cooling the upper ocean and elevating the thermocline in the equatorial Pacific.

Addressing the full role of ITF in the ocean–atmosphere coupled climate requires experiments with coupled general circulation models (CGCMs). Two recent studies explore the role of ITF using CGCMs. Schneider (1998, hereafter S98) uses the ECHAM and the Hamburg Ocean Primitive Equation (HOPE) (ECHO) model developed at the Max-Planck-Institut für Meteorologie, and conducts a 10-yr couplet of experiments (one with ITF open and the other with ITF closed). Wajsowicz and Schneider (2001, hereafter WS01) perform similar numerical experiments for 20 yr in the Center for Ocean–Land–Atmosphere Studies coupled model. The role of ITF in regulating the mean subsurface oceanic states in these two CGCM studies qualitatively agrees with that in the above-mentioned ocean general circulation model (OGCM) studies. In addition to the direct oceanic effects, the CGCM experiments found that the ITF regulates the position of the atmospheric deep convection, and, in turn, the global atmospheric pressure field and surface wind patterns by affecting the position and size of the oceanic warm pool. These atmospheric changes feed back onto the oceanic changes, extending the influence of ITF through the entire Tropics, and even globally. Because in both S98 and WS01 the models are integrated over a relatively short period of time (10 yr in S98 and 20 yr in WS01), only the effects of ITF on the mean climate are examined, and the ITF effects on the climate variability of the Indo–Pacific have not been addressed thus far.

In this study we explore the effects of ITF with a state-of-the-art global coupled ocean–atmosphere–land–ice model recently developed at the Geophysical Fluid Dynamics Laboratory (GFDL) of U.S. National Oceanic and Atmospheric Administration (NOAA). This study builds on the results of S98 and WS01, and the previous ocean-only model research. However, we integrate control and perturbation experiments with the CGCM for 200 yr, which allows us to explore the influence of ITF closure on the mean tropical Indo–Pacific climate, on the interannual variability of the Indo-Pacific, and on the extent to which changes in variability rectify into mean-state changes.

The paper is organized as follows. The GFDL Coupled Climate Model version 2.1 (CM2.1) and numerical experiment procedure are described in section 2, and the model simulation of the Indian–ITF–Pacific climate system in the control experiment is presented in section 3. The effects of the ITF on the mean climate are shown in section 4. The changes in the interannual variability of the Indo–Pacific domain in response to the closure of ITF are examined in section 5. Implications and limitations of our results are discussed in section 6, and a summary is presented in section 7.

2. Model description and experiments

The model used in this study is the GFDL CM2.1 global coupled atmosphere–ocean–land–ice model. Details of model formulation are documented in Gnanadesikan et al. (2006; ocean model), GFDL Global Atmospheric Model Development Team (2004; atmosphere model), Delworth et al. (2006; coupled model), Stouffer et al. (2006; climate sensitivity), Wittenberg et al. (2006; Pacific Ocean), and Song et al. (2007; Indian Ocean). Only a brief description of the coupled model configuration is provided here. This is one of the models used by NOAA/GFDL in its contributions to the Fourth Assessment Report (AR4) of the Intergovernmental Panel on Climate Change (IPCC). Recent model intercomparison studies (e.g., Saji et al. 2006) find that CM2.1 is one of the best in simulating the Indo–Pacific.

The ocean component of the CM2.1 coupled model is based on the GFDL Modular Ocean Model version 4. The model ocean has 50 vertical layers with 10-m resolution in the upper 220 m. The ocean horizontal resolution is $1^\circ \times 1^\circ$, and the meridional grid spacing gradually reduces to $1/3^\circ$ at the equator. Diurnal insolation is used to force the ocean model, and shortwave penetration depth depends on a prescribed spatially varying climatological ocean color field. The model has an explicit free surface, with true freshwater fluxes between the ocean, land, cryosphere, and atmosphere. The mixed layer is predicted using the K-profile vertical mixing scheme (Large et al. 1994). The eddy-mixing parameterization of Gent and McWilliams (1990) as implemented by Griffies (1998) is used in the model.

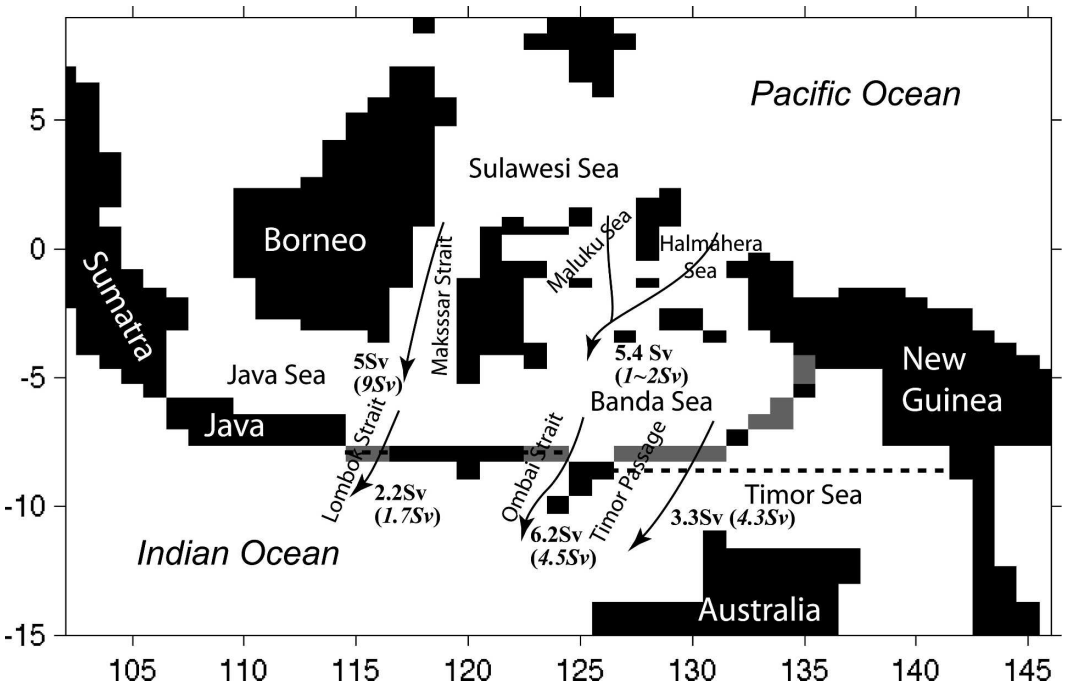

FIG. 1. Model land–ocean configuration in the Indonesian Seas. The gray blocks are the ocean grid points that are replaced by land grid points in order to block the ITF. The dashed lines are the path along which the total ITF transport is calculated. The model-simulated annual mean depth-integrated transports through various channels, as well as those estimated from observations (italic in parentheses), are shown. The observational estimates are adopted from Gordon (2001, and references therein).

The atmosphere component is the GFDL atmosphere model AM2p12b (GFDL Global Atmospheric Model Development Team 2004). The model has 24 vertical layers and 2° latitude × 2.5° longitude horizontal spacing. A K-profile planetary boundary layer scheme, a relaxed Arakawa–Schubert convection, and a parameterization of the vertical momentum transport by cumulus convection are employed in the model.

Different components of the GFDL CM2.1 model are coupled through the flexible modeling system (V. Balaji et al. 2006, personal communication). The atmosphere, ocean, land, and sea ice exchange fluxes every 2 h and all fluxes are conserved within machine precision.

We explore the role of ITF in the climate by comparing the two experiments. In both experiments the 1990 values of trace gases, insolation, aerosols, and land cover are specified. The control experiment (hereafter CTRL) is initialized at year 001 as described in Delworth et al. (2006), and then integrated forward in time through year 300. The tropical Indo–Pacific characteristics of the CTRL are discussed fully in Wittenberg et al. (2006) and Song et al. (2007). In the perturbation experiment (hereafter NOITF), the Lombok Strait, the Ombai Strait, and the Timor Passage are blocked by land bridges (shown in Fig. 1 as gray blocks). NOITF is initialized using the output of the CTRL run at the end of year 100 and is integrated for another 200 yr. In this study we analyze the 200-yr simulation in NOITF and the last 200-yr (of the total 300 yr) simulation in CTRL.

3. Features of model simulation

In CTRL, the model produces a realistic simulation of various aspects of the global climate (e.g., Gnanadesikan et al. 2006; GFDL Global Atmospheric Model Development Team (2004; Delworth et al. 2006; Stouffer et al. 2006; Wittenberg et al. 2006; Song et al. 2007). Here we only briefly comment on the representation of the tropical Indian and Pacific Oceans (for details see Song et al. 2007; Wittenberg et al. 2006) and the ITF in CTRL.

Many features of the simulated equatorial Pacific annual mean SST, thermocline depth, and Equatorial Undercurrent are reasonably realistic (Wittenberg et al. 2006). The model reproduces a westward-propagating annual cycle of SST and zonal winds along the equator, consistent with observations. The model has a robust ENSO with irregular period between 2 and 5 yr, substantial multidecadal fluctuation in amplitude, a distribution of SST anomalies that is skewed toward warm events, and a realistic evolution of subsurface temperature anomalies. However, the following biases that are

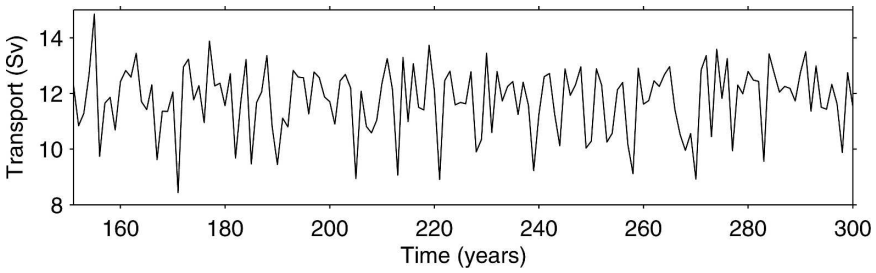

FIG. 2. Annual mean ITF transport in the CTRL run. The ITF transport is computed as the sum of the depth-integrated ITF transport through the Lombok Strait, the Ombai Strait, and the Timor Passage (i.e., along the dashed lines shown in Fig. 1).

common to many CGCMs are also present in CTRL: the mean SST along the equatorial Pacific is 1°–2°C too cold, the mean trade winds and atmosphere deep convection are shifted westward, the mean equatorial thermocline is too diffuse, and the tropical precipitation anomalies during ENSO are shifted westward.

In the Indian Ocean CTRL reasonably simulates both the monsoon wind reversal and the seasonal cycle of SST and surface ocean currents (Song et al. 2007). The model reproduces the semiannual cycle of the equatorial zonal winds and the equatorial thermocline depth, and the Wyrtki (1973) jets during the monsoon transition seasons. The annual mean equatorial Indian Ocean thermocline in the model is tilted downward toward the east, consistent with observations. The model successfully simulates the ENSO-induced interannual SST variability in the Indian Ocean, and the so-called Indian Ocean dipole/zonal mode (IODZM) events (Saji et al. 1999; Webster et al. 1999). The statistical relationship between the interannual Indian Ocean variability and ENSO in the model agrees with observations. Yet, there are several unrealistic aspects in the Indian Ocean, including cooler mean SST, stronger surface winds, and more equatorially confined precipitation.

The model ocean grid is constructed to resolve the major channels within the Indonesian Sea region (Fig. 1). We calculate the total ITF volume and heat transport as the sum of depth-integrated ITF transport through the three southernmost channels of the Indonesian Seas (i.e., the Lombok Strait, the Ombai Strait, and the Timor Passage) and the vertical profiles of ITF as the average of the three channels, along the dashed lines in Fig. 1. The annual mean total ITF volume transport into the Indian Ocean in the model is 11.7 Sv, with a heat transport of 0.75 PW [a reference temperature of 3.4°C is used, after Vranes et al. (2002)], both of which are well within the previously estimated ranges of 5–20 Sv and 0.5–1.0 PW (see Godfrey 1996; Gordon 2001, 2005 for reviews and references therein). The seasonal variation of the model ITF volume transport agrees with observations (Meyers et al. 1995), with a maximum of 14.1 Sv in August and a minimum of 9.4 Sv in February. The model-simulated annual mean ITF volume transport has interannual variability (Fig. 2) and a standard deviation of 1.2 Sv. Consistent with studies based on expendable bathythermograph (XBT) measurements (Meyers 1996) and an ocean data assimilation product (England and Huang 2005), the interannual variation of the ITF transport is significantly correlated with that of Niño-3 SST, with a correlation coefficient of −0.42 between the monthly ITF transport anomalies and Niño-3 SST anomalies (i.e., less ITF transport during periods of anomalous warm Niño-3 SST). The bulk of the ITF transport is concentrated in the upper 500 m (Fig. 3a), consistent with observations (e.g., Gordon et al. 1999; Vranes et al. 2002). The temperature T and salinity S profiles of ITF in the model (Figs. 3b–c) also agree with available measurements (e.g., Vranes et al. 2002; Ffield and Gordon 1992; England and Huang 2005), except that the surface layer is too fresh. We also show in Fig. 1 the depth-integrated volume transport through various channels, along with transport estimates from observations. The ITF transport partition among channels is consistent with observational estimates, except that the model simulates too much southward transport through the Maluku Sea and the Halmahera Sea, whereas there is too little through the Makassar Strait.

4. ITF effects on mean states

Now we show the differences in mean states between the NOITF and CTRL runs, and compare our results with previous OGCM (e.g., Hirst and Godfrey 1993; Murtugudde et al. 1998; Lee et al. 2002) and CGCM studies (S98; WS01). For the sake of such a comparison, the mean states discussed in this section are simply defined as a time average, specifically, over the last 180 yr of the 200-yr simulation, to avoid initial adjustment. However, as we show in section 5, aspects of the mean-

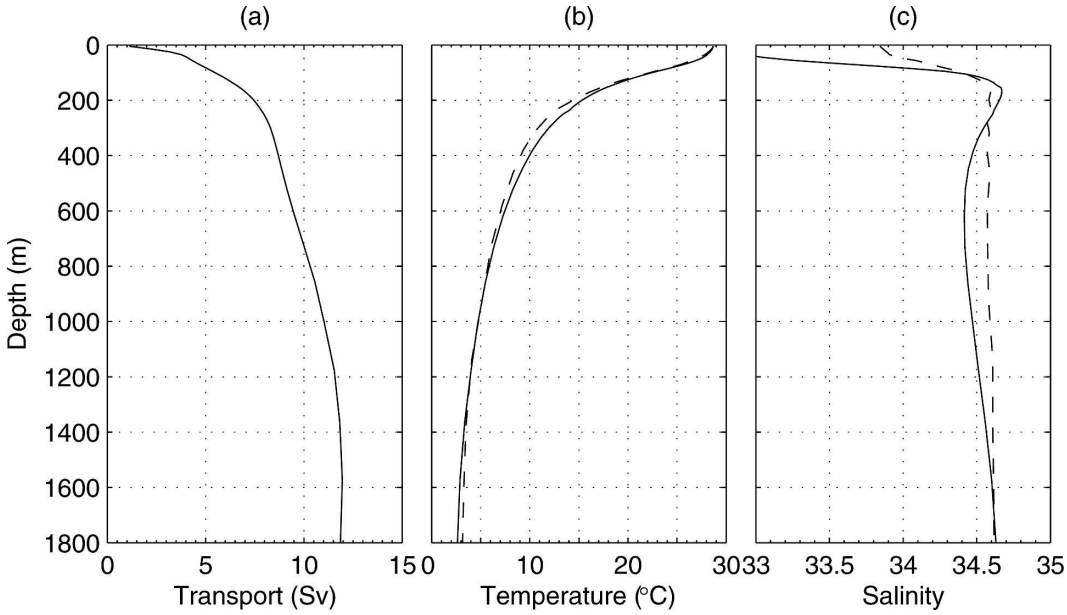

FIG. 3. Vertical profiles of the ITF (a) volume transport (integrated from the sea surface downward), (b) temperature, and (c) salinity from the model simulation (solid curves) and from the Simple Ocean Data Assimilation product (only *T*–*S* profiles are shown; Carton et al. 2000a,b; dashed curves). The vertical ITF profiles are computed as the average of the Lombok Strait, the Ombai Strait, and the Timor Passage (i.e., along the dashed lines shown in Fig. 1).

state differences between the ITF-on and -off scenarios arise from changes in the character of the interannual variability in the tropical Indo–Pacific. This issue is further discussed in section 6. Figure 4 displays changes to annual mean fields resulting from the closure of ITF (shown as NOITF minus CTRL), and each subsection below refers to a particular panel of Fig. 4. Changes to seasonal mean states are noted whenever needed.

a. Barotropic streamfunction (Fig. 4a)

The most direct consequence of the closure of ITF occurs to the ocean circulation. Consistent with previous OGCM and CGCM studies, the NOITF minus CTRL difference in barotropic streamfunction is characterized by an anomalous clockwise circulation, encompassing the southwestern Pacific and most of the Indian Ocean. The anomalous circulation represents the reduced volume transport of the South Equatorial Current, the Agulhas Current, and the Agulhas Retroflection in the Indian Ocean, and increased volume transport of the southward-flowing East Australian Current in the Pacific. These changes to ocean circulation agree with previous OGCM and CGCM studies.

b. Upper-ocean heat content (Fig. 4b)

Throughout this paper, the upper-ocean heat content is calculated as the temperature averaged in the upper 300 m. Figure 4b shows that the upper-ocean heat content in the Indian Ocean is reduced (i.e., thermocline is elevated), consistent with the conclusion from previous studies that the closure of ITF cools the upper Indian Ocean. Figure 4b also shows that the closure of ITF acts to warm the upper eastern equatorial Pacific (EEP) and the coast of South America, but cool the upper western equatorial Pacific. In fact, the heat content (0–300 m) of the tropical Pacific (10°S–10°N, 140°E–70°W) is slightly less in the NOITF run than in the CTRL run. The zonally asymmetric response of the upper-ocean heat content of the tropical Pacific to the closure of ITF in our model disagrees with previous OGCM and CGCM studies, which show warming through the entire tropical Pacific although some of them (e.g., Lee et al. 2002; S98; WS01) display stronger warming in the eastern Pacific. The difference from the OGCM studies (e.g., Lee et al. 2002) may be attributed to ocean–atmosphere coupling, because we see in section 4h that mean trade winds in the Pacific are weakened due to the closure of ITF, which relaxes the zonal slope of the equatorial Pacific thermocline and tends to shoal the thermocline across the Pacific (Jin 1997; Vecchi et al. 2006).

We further note that the upper-ocean stratification in the eastern tropical Indian Ocean (ETIO) is reinforced, whereas that in the equatorial Pacific is weakened in response to the closure of ITF (not shown), because the ITF thermocline water remains in the Pacific rather than flowing to the Indian Ocean. The changes to ther-

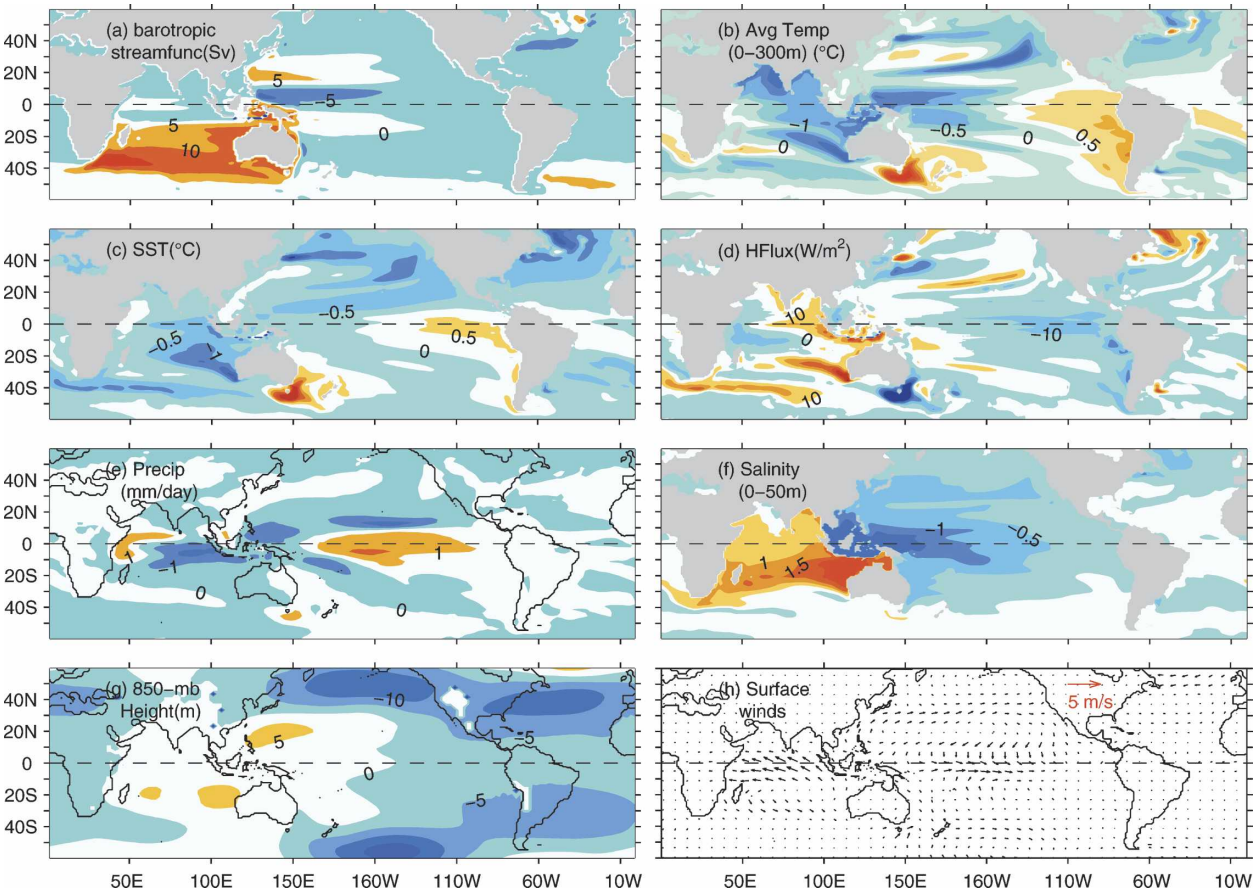

FIG. 4. Annual mean differences, NOITF minus CTRL. All noticeable features are significant at 95% level. (a) Larger streamfunction values are on the right-hand side of the circulation. (f) The average salinity in the upper 50 m.

mocline depth and upper-ocean stratification resulting from the closure of ITF affect ocean–atmosphere coupled variability (especially in the eastern tropical Indian Ocean), which we shall discuss in detail in section 5.

c. Sea surface temperature (Fig. 4c)

In response to the closure of ITF, SST becomes warmer in the eastern equatorial Pacific, off the west coast of South America and southeast of Australia, while it becomes cooler across most of the Indian Ocean, the western equatorial Pacific, the Agulhas Retroflection region, and the North Pacific and North Atlantic Oceans. As a consequence, the mean zonal SST gradient across the equatorial Pacific is reduced. Several discrepancies from S98 and WS01 are noted as follows: the center of warming in the eastern equatorial Pacific is located at about 110°W, which is east of that shown in those two studies; the magnitude of the warming is weaker in our model; the magnitude of cooling in the eastern tropical Indian Ocean is comparable with that of WS01, but is larger than that of S98; and the surface cooling in the North Pacific and North Atlantic is stronger than in either of the two previous studies. Nevertheless, the principal character of the changes is consistent in all three CGCM studies.

d. Net surface heat flux (Fig. 4d)

The response of net surface heat flux across the atmosphere–ocean interface in the Tropics generally acts to counterbalance SST changes, in agreement with other studies (Hirst and Godfrey 1993; S98; WS01). In addition, the seasonality of changes to net surface heat flux matches that of SST (not shown). The change in net surface heat flux is mostly due to changes in shortwave radiation and latent heat flux. Changes in shortwave radiation (Fig. 5a) arise from the changes in cloud cover, and have a spatial pattern similar to that of precipitation (Fig. 4e), except in regions of the south tropical Indian Ocean west of Australia and the south tropical Pacific west of south America, where the effects of trade cumulus and low-level stratus could be important,

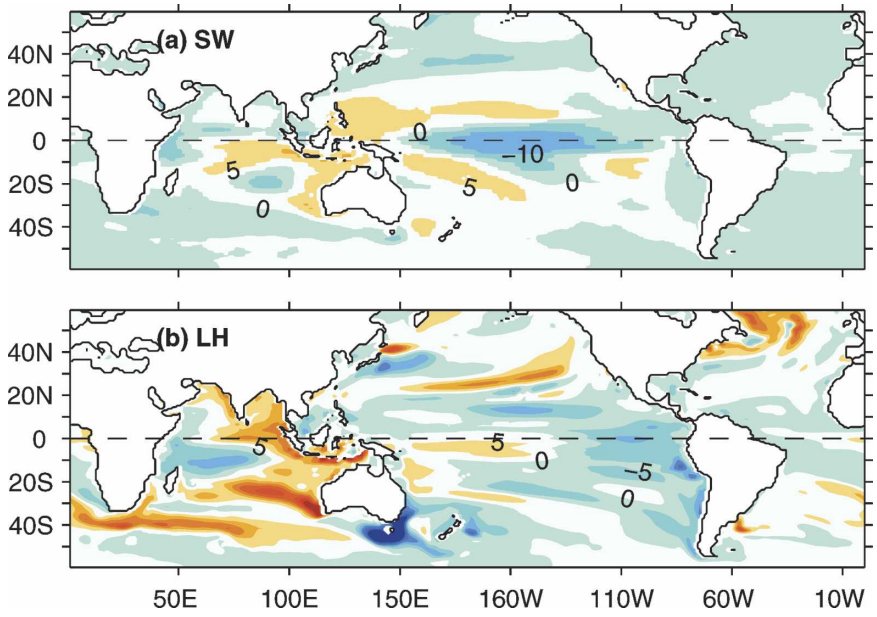

FIG. 5. Annual mean differences (NOITF minus CTRL) of (a) shortwave radiation and (b) latent heat (positive values into the ocean).

respectively. Changes in latent heat flux are mostly due to SST changes, and are most noticeable in the eastern Indian Ocean where SST changes are the largest (Fig. 5b). The feedback coefficient between SST and surface heat flux has been estimated in a number of studies (e.g., Haney 1971; Kleeman and Power 1995). In our model the globally averaged SST damping coefficient resulting from net surface heat flux and latent heat flux are estimated to be -13 and -7.4 W m^{-2} °C^{-1}, respectively. There is qualitative agreement in the spatial pattern of changes in net surface heat flux between S98, WS01, and the present study. The magnitude of the changes in the tropical Pacific Ocean in our study and S98 is less than that in WS01, resulting from larger SST differences in WS01.

e. Precipitation (Fig. 4e)

Changes in tropical SSTs affect the distribution of tropical precipitation. As SST becomes warmer in the eastern tropical Pacific and cooler in the western tropical Pacific and eastern Indian Ocean, the tropical deep convection shifts away from the Maritime Continent; and consequently there is reduced rainfall in the eastern tropical Indian Ocean, increased rainfall in the central/eastern equatorial Pacific, and a southward shift of the intertropical convergence zone (ITCZ). Meanwhile, there are anomalous low-level convergent winds (section 4h) over the western Indian Ocean in NOITF, which induces anomalously above-normal rainfall there. Both S98 and WS01 show a similar eastward shift of the deep convection. However, the center of the precipitation anomaly is west of the center of the warm sea surface temperature anomaly (SSTA) in the equatorial Pacific in our model, whereas the two centers are more or less at the same longitude in WS01. That could be due to the fact that the location of the deep convection in the CTRL run is too far west compared with observations.

f. Salinity (Fig. 4f)

The source waters of the ITF are principally the low-salinity North Pacific thermocline and intermediate waters (Gordon 2001). Hence, when the ITF passages are closed these relatively fresh waters, as well as the low-salinity surface water from the Indonesian Seas, are diverted to the equatorial Pacific, which decreases the salinity of the Pacific and increases the salinity of the Indian Ocean. We note that the salinity pattern shown in Fig. 4f is dissimilar to that of precipitation (Fig. 4e), and also to that of evaporation–precipitation (not shown). That suggests that changes in net surface freshwater flux play a minor role in determining the salinity difference shown in Fig. 4f. The closure of the ITF also affects the vertical distribution of salinity as follows: the vertical salinity gradient in the upper western Pacific is reinforced, whereas that in the eastern Indian Ocean is reduced. In addition, the thickness of the barrier layer (Lukas and Lindstrom 1991) in both the western equa-

torial Pacific and Indian Ocean is reduced (not shown), because of the dominant role of the shallower thermocline in these regions in determining the change in barrier layer.

g. Atmospheric pressure (Fig. 4g)

At 850-mb there are anomalous highs in the southern subtropical Indian Ocean and northwestern tropical Pacific Ocean, and zonally extended troughs in the high latitudes of both hemispheres. Those changes to atmospheric pressure resemble the atmospheric pressure responses to El Niño–like SST and precipitation conditions in the equatorial Pacific, as shown in studies of ENSO teleconnection (Lau and Nath 2003; Seager et al. 2003; Lau et al. 2005). The changes in atmospheric pressure qualitatively agree with WS01, but with smaller magnitudes. S98 finds changes with zonal wavenumber 2, which contrasts with both WS01 and this study.

h. Surface winds (Fig. 4h)

The response of surface winds to the closure of ITF is characterized by weaker trade winds in the tropical Pacific, and anticyclonic circulation in the southern Indian Ocean and midlatitudes of the north Pacific, as expected from the eastward shift of atmospheric deep convection and the associated changes in atmospheric pressure field. The relaxed trade winds of the Pacific are consistent with the flatter mean thermocline of the equatorial Pacific in NOITF.

5. ITF effects on the interannual variability

Now we investigate the response of the interannual variability of the tropical Indo–Pacific to the closure of ITF. We first identify the regions where the intensity of SST variability changes by comparing the standard deviation of monthly SST in the NOITF and CTRL runs (Fig. 6). It is conspicuous that the interannual variability of SST in the NOITF run becomes considerably stronger in EEP and ETIO, which are the action centers of ENSO and the IODZM, respectively. We now focus on the two regions where SST variability is enhanced in the NOITF run.

a. Pacific Ocean variability

The enhanced SST variation in EEP indicates intensified ENSO variability. We use the Niño-3 index (SST averaged over the area 5°S–5°N, 150°–90°W) as a proxy for ENSO variability. Using the Niño-3.4 index does not change the results. We examine the Niño-3 SST, instead of the SST anomaly, because the seasonal cycle

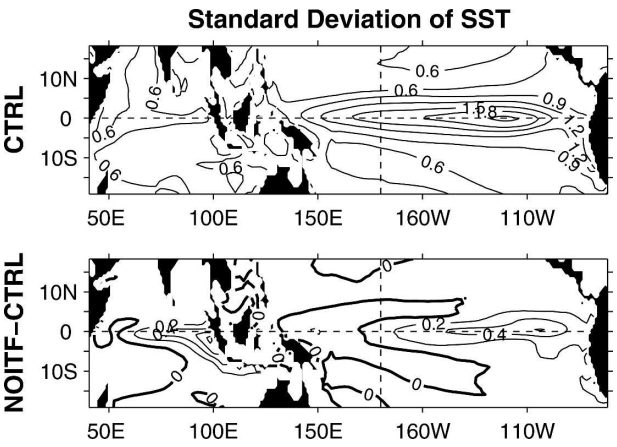

FIG. 6. Std dev of monthly SST over the 200-yr simulations.

in NOITF includes the information of ENSO behavior change. The power spectra of the monthly Niño-3 SST index from the two experiments are shown in Fig. 7. In CTRL there is a broad peak in the interannual band of 3–7 yr, with a maximum around the period of 4 yr. In response to the closure of ITF, the amplitude of the spectral peak in the interannual band becomes larger, suggesting stronger ENSO variability; the peak also becomes narrower with maximum around the period of 3 yr, indicating more regular ENSO variability.

The histograms of Niño-3 SST from the two experiments are shown in Fig. 8a. The main difference between the two histograms is that the NOITF distribution has two peaks, with the primary peak corresponding to the most likely SST values of CTRL and the secondary peak indicating more extreme warm SST anomalies. Meanwhile, the time series of Niño-3 SST in the two experiments (Fig. 9) show that it is warm ENSO events that occur more frequently and have larger amplitudes in the NOITF scenario, while cool ENSO events do not undergo comparable intensification. We also notice, qualitatively, that the most likely SST values in NOITF and those in CTRL are similar, suggesting that the mean-state differences in the Niño-3 region shown in Fig. 4c could be interpreted as arising from the rectification of more intense and frequent El Niño events.

We examine more quantitatively to what extent the enhanced ENSO variability affects the mean Niño-3 SST difference. The mean Niño-3 SST in NOITF calculated as simple time average is 26.1°C (i.e., mean of the distribution represented by gray shades in Fig. 8a), which is 0.5°C higher than the mean of 25.6°C in CTRL (i.e., mean of the distribution represented by black border lines in Fig. 8a). To eliminate the contribution of the secondary peak in the NOITF distribution to its

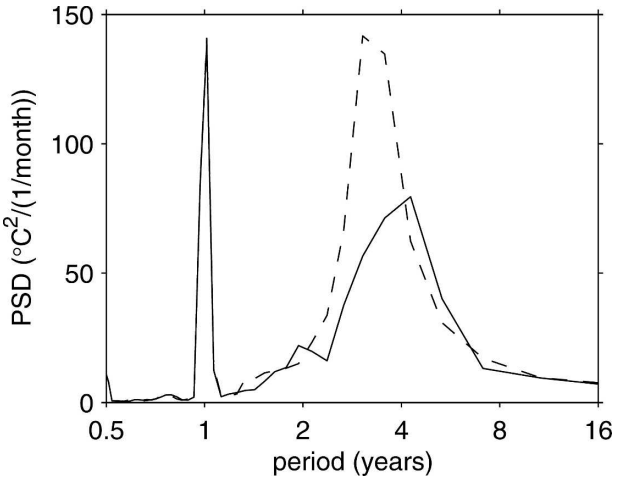

FIG. 7. Power spectrum density of monthly Niño-3 SST in the CTRL (solid) and NOITF (dashed) runs.

mean, we recalculate the mean Niño-3 SST in NOITF using Niño-3 SSTs from NOITF that are less than 28°C and Niño-3 SSTs from CTRL that are greater than 28°C. That is, we calculate the mean of the combined distribution, which in Fig. 8a comprises gray shades to the left of the 28°C mark and black border lines to the right of the 28°C mark. The resultant mean Niño-3 SST is 25.7°C, only 0.1°C higher than the mean of 25.6°C in CTRL. It suggests that most of the mean SST warming in EEP shown in Fig. 4c arises from the changes in El Niño behavior. Using the same technique we find that most of the mean differences in precipitation and surface winds in the Pacific can also be attributed to intensified El Niño events. However, for the mean difference in the upper-ocean heat content, a substantial portion is not a result of the differences in interannual variability, because simple shifts of the peaks of the histograms of the upper-ocean heat content in the equatorial Pacific are clearly seen in Figs. 8b–c. This is consistent with the results from previous OGCM studies (e.g., Hirst and Godfrey 1993; Godfrey 1996; Murtugudde et al. 1998; Lee et al. 2002) in which the direct consequence of the closure of ITF, without air–sea feedback, is to change the thermocline configuration.

Now we perform a composite analysis to explore the changes in the structure of El Niño events between the ITF open and closed scenarios. Because the differences between the climatologies of the two experiments are largely due to changed interannual variability, we use the climatology of CTRL to calculate the anomalies associated with El Niño in both experiments. We identify El Niño events as times in which Niño-3 SST exceeds 27.5 for 6 months in both ITF open and closed scenarios. According to this criterion, there are 33 and 65 El Niño events in CTRL and NOITF, respectively.

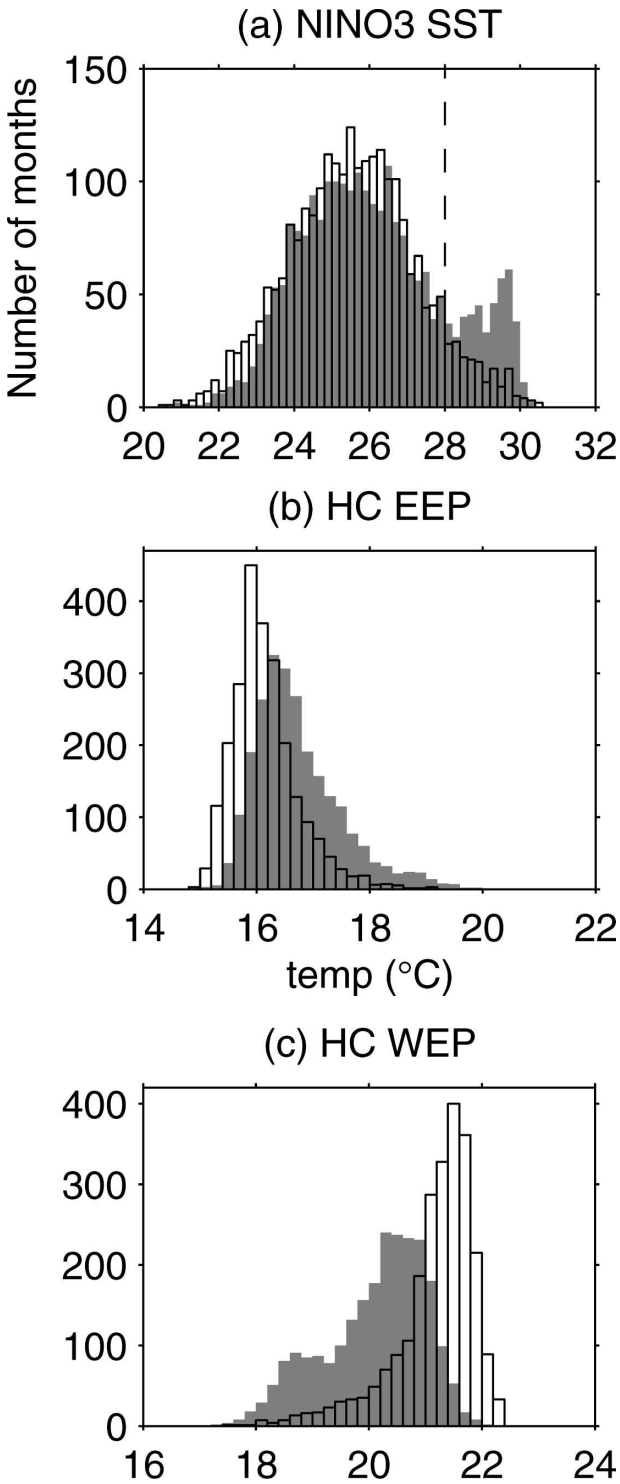

FIG. 8. Histograms of monthly (a) Niño-3 SST, (b) ocean heat content (0–300 m) of the eastern equatorial Pacific (10°S–10°N, 140°–80°W; the region where heat content is increased in NOITF as shown in Fig. 3b), and (c) ocean heat content of the western equatorial Pacific (10°S–10°N, 150°–160°W; the region where heat content is reduced in NOITF as shown in Fig. 3b) in the CTRL (black border lines) and NOITF (gray shades) runs. The position of 28°C is marked in (a) (see section 5a for details).

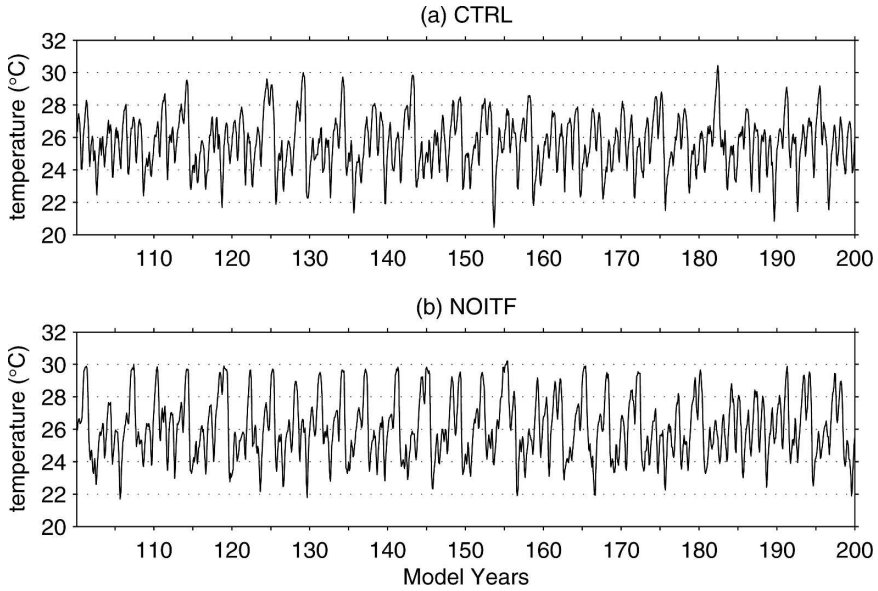

FIG. 9. Time series of monthly Niño-3 SST in (a) CTRL and (b) NOITF runs. Only the last 100 yr are shown.

The composite anomalies of SST and precipitation from boreal summer [June–August (JJA)] of the El Niño years (year 0) to boreal spring [March–May (MAM)] of the following years (year + 1) are shown in Fig. 10. In early stages of ENSO evolution [MAM(0) and JJA(0)], the spatial patterns of SST and precipitation anomalies in the two experiments are similar, but with a significantly larger amplitude in NOITF. In particular, the SST warming during this time along the coast of South America in NOITF is more noticeable. During the peak of warm ENSO events [DJF(0)], the SST and precipitation anomalies in NOITF are shifted eastward, relative to those in CTRL. Furthermore, the relative longitudinal positions of SST and precipitation also differ in the two experiments; the maximum of the precipitation anomalies is roughly at the same longitude as the maximum of the SSTA (~110°W) in NOITF, whereas it is located to the west of the maximum of SSTA in CTRL. The eastward shift of precipitation anomalies in NOITF is likely due to the even more reduced SST gradient at the equator during the peak of warm ENSO events. The differences seen in DJF(0) persist in MAM(+1), but are less pronounced.

The zonal wind anomalies closely correlate with precipitation anomalies. It is shown in Fig. 11 that in NOITF anomalous surface westerlies extend further east in NOITF and have a larger meridional extent, especially during the DJF(0) and MAM(+1) seasons. The eastward shift of the westerly anomalies and the meridional expansion of the westerly anomalies have been shown to be associated with stronger ENSO (An and Wang 2000; Vecchi 2006). An and Wang (2000) indicate that such changes in the structure of westerly anomalies should be associated with a longer ENSO period, which is contrary to what we see in NOITF (Fig. 7). This discrepancy suggests that other changes resulting from the closure of ITF, such as changes in background ocean stratification (e.g., Fedorov and Philander 2000; Wittenberg 2002, 2004), also play a role in determining ENSO behavior. One anonymous reviewer proposes another possible mechanism influencing ENSO periodicity. When the ITF is closed, the all of the Mindanao Current, instead of a fraction of it, converges into the western equatorial Pacific. As a result, the recharge of the discharge–recharge mechanism should be increased, which deepens the thermocline of the equatorial western Pacific faster and hence lead to a new ENSO event faster.

Beginning in December–February (DJF), the El Niño composite central Pacific zonal wind and precipitation anomalies for both CTRL and NOITF shift from being centered about the equator to being centered south of the equator (Fig. 11), which also happens in the observational record (e.g., Harrison 1987; Harrison and Vecchi 1999; Larkin and Harrison 2002; Vecchi and Harrison 2003, 2006). It has been suggested that this southward shift of winds anomalies arises from the annual cycle of insolation, and drives a shoaling of the eastern equatorial Pacific thermocline that preconditions the termination of El Niño events (Harrison and Vecchi 1999; Vecchi and Harrison 2003, 2006). In both the CTRL and NOITF composites, the east Pacific

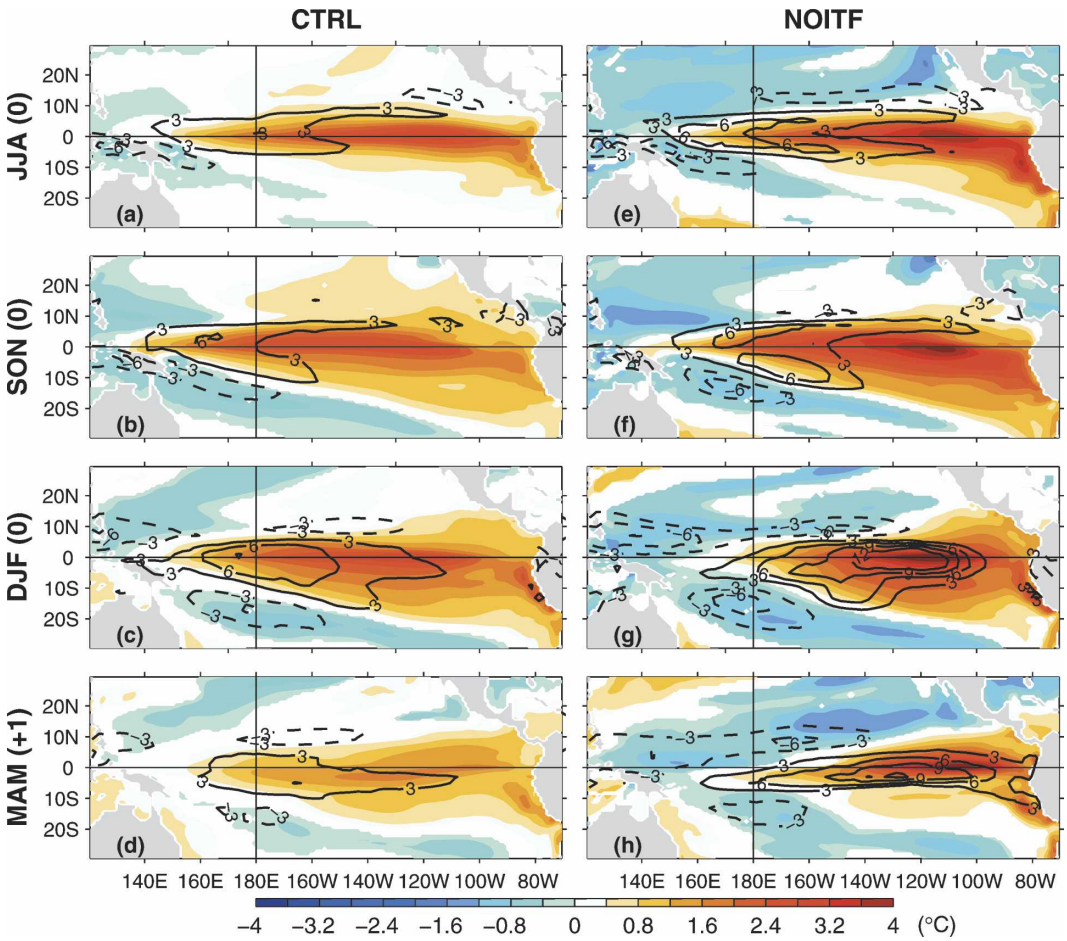

FIG. 10. El Niño composite anomalies of SST (color) and precipitation [mm day^{-1}; contour; solid (dashed) lines denote positive (negative) values] in the NOITF and CTRL runs. The climatology of CTRL is used when calculating the anomalies in both ITF open and closed scenarios. Only values significant at 95% level are plotted.

thermocline begins to shoal in early boreal winter (Fig. 12), consistent with this proposed mechanism.

It has also been suggested that the termination of extremely large El Niño events should be distinct from that of moderate El Niño events, with warm eastern equatorial Pacific SST anomalies persisting into boreal spring in spite of a shoaling local thermocline (Vecchi and Harrison 2006; Vecchi 2006). Vecchi and Harrison (2006) and Vecchi (2006) suggest that in extreme El Niño events, the development of an equatorial ITCZ from late boreal winter through boreal spring weakens the local easterly winds and decouples the cooling subsurface from the warm SST anomalies, and only when the ITCZ retreats north of the equator and easterlies return do SSTs cool. Interestingly, the termination of the large-amplitude composite El Niño events in NOITF exhibits these characteristics, and they are distinct from those in CTRL (Figs. 11, 12). In CTRL, composite zonal wind and precipitation anomalies are confined to the western and central Pacific (Figs. 11, 12), and east Pacific SSTs cool as the thermocline shoals in boreal winter (Fig. 12). Meanwhile, in boreal spring of NOITF precipitation moves onto the eastern equatorial Pacific and local zonal winds weaken (Figs. 11, 12). The NOITF composite SST remains warm in boreal winter in spite of a cooling subsurface (Fig. 12), but cools rapidly as the local easterlies return in May/June SST. We suggest that some of the warming in Niño-3 in response to the closure of ITF (Fig. 8) results from the difference in the termination of CTRL and NOITF El Niño events.

The modeled changes in ENSO behavior from the closure of the ITF raise the immediate question, why? The closure of ITF causes a variety of changes that could potentially influence ENSO (such as climatologies of the equatorial Pacific), and the mean and variability of the Indian Ocean (the relationship between the Indian Ocean conditions and ENSO is still an on-

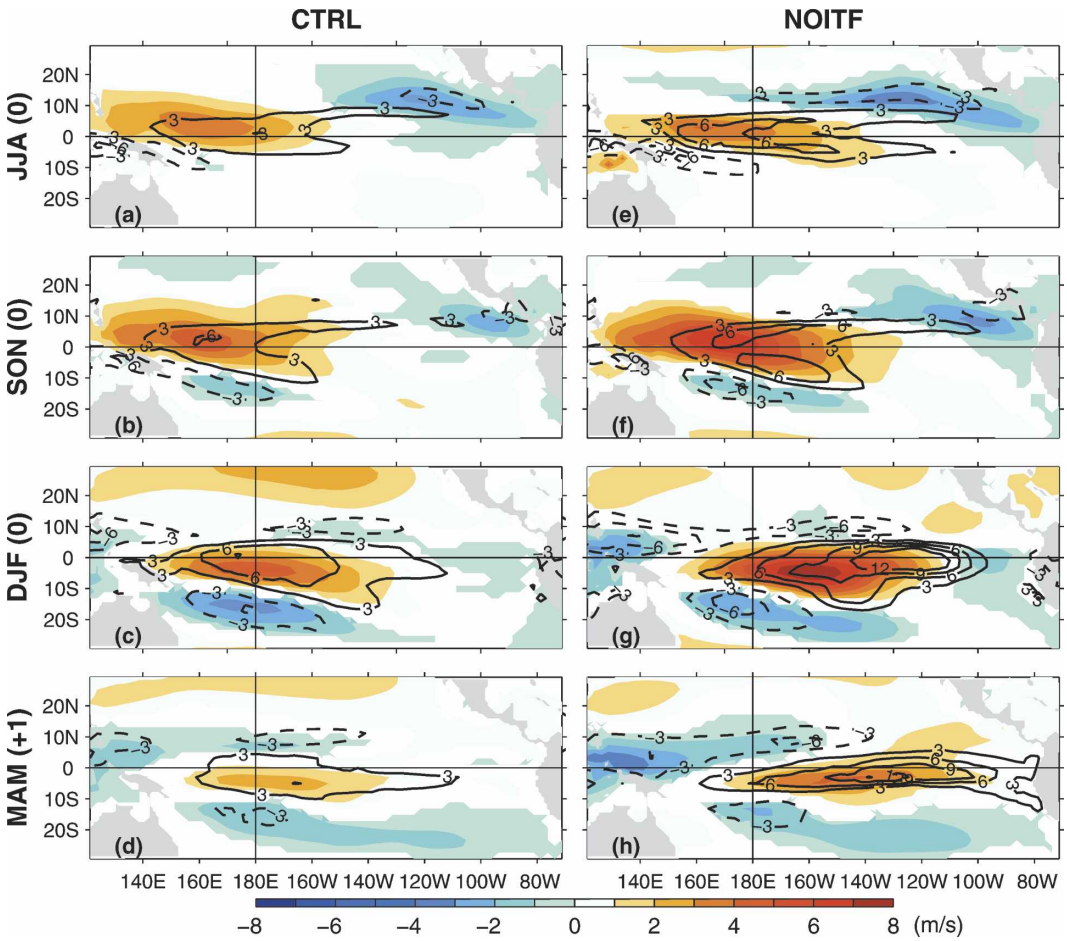

FIG. 11. El Niño composite anomalies of zonal wind (color) and precipitation [mm day^{-1}; contour; solid (dashed) lines denote positive (negative) values] in the NOITF and CTRL runs. The climatology of CTRL is used when calculating the anomalies in both ITF open and closed scenarios. Only values significant at 95% level are plotted.

going research topic). Therefore, additional perturbation numerical experiments from a suite of models of varying complexity are necessary to isolate the effects of each of those factors to decipher the ITF–ENSO relationship. Such a modeling effort is substantial and we leave it to future studies.

b. Indian Ocean variability

In NOITF, there is prominent enhancement in the interannual SST variability of the Indian Ocean (Fig. 6), especially in the eastern Indian Ocean along the coast of Java–Sumatra. The ETIO is one of the few regions of the Indian Ocean where significant atmosphere–thermocline coupled feedback can occur (e.g., Annamalai et al. 2003; Annamalai and Murtugudde 2004; Murtugudde and Busalacchi 1999; Wajsowicz 2004). Recently, the region has drawn much attention because it is recognized as one of the action centers of the IODZM (e.g., Saji et al. 1999; Webster et al. 1999; Gualdi et al. 2003; Huang and Kinter 2002; Lau and Nath 2004; Li et al. 2003; Murtugudde et al. 2000), which is characterized by the east–west contrasting SST anomalies, particularly during boreal fall. The western tropical Indian Ocean (WTIO), the other center of IODZM, does not exhibit corresponding enhancement in SST variability. In addition, in NOITF the correlation between the SSTAs in ETIO and WTIO becomes much weaker during September–November (SON) (−0.13 in NOITF versus −0.50 in CTRL). Thus, in the NOITF scenario simulated in the GFDL coupled model, the SSTs of WTIO and ETIO do not oscillate as a seesaw, even during SON when IODZ anomalies peak. In this section we principally focus on the variability in ETIO, which (as shown below) results from amplified local atmosphere–thermocline feedbacks that lead to extreme anomalous cooling.

The time series of SST in ETIO (10°S–0°, 90°–110°E) in the two experiments are exhibited in Fig. 13. In

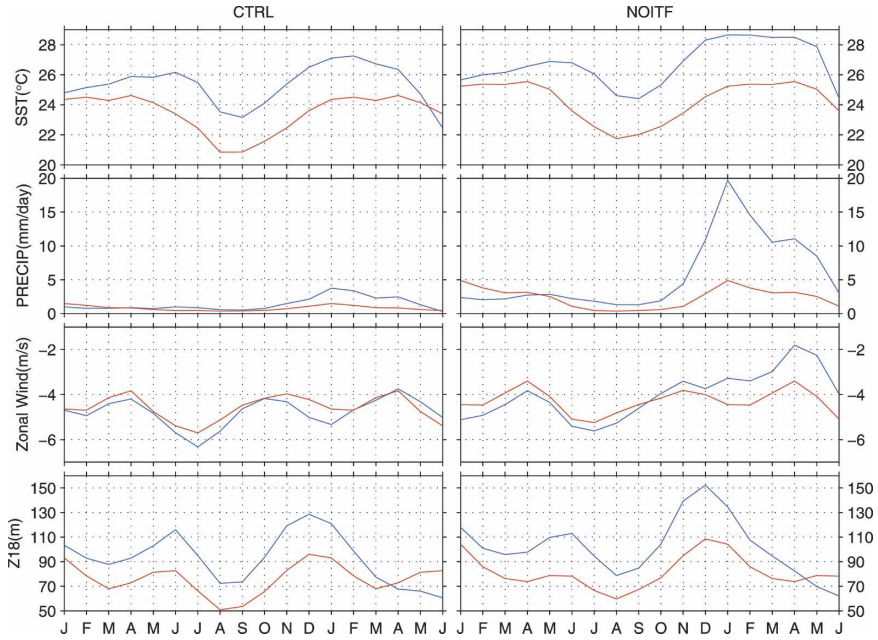

FIG. 12. El Niño composite total values (blue curves) of SST, precipitation, surface zonal wind, and Z18 (depth of the 18°C isotherm) averaged between 5°S–5°N, 110°–120°W in CTRL and NOITF. The red curves are climatological values in the corresponding experiment.

CTRL (as in the observations), there is prominent interannual SST variability in the ETIO, characterized by anomalous cooling during certain years (Fig. 13a); the evolution of these model events has been documented in detail in Song et al. (2007). These anomalous SST cooling events in ETIO (referred to as "ETIO cooling" hereafter) have been studied as a component of the IODZM using both observations and numerical models (see Yamagata et al. 2004, and references therein), and involve atmosphere–thermocline coupled feedbacks. In both the observations and CTRL, ETIO cooling has pronounced seasonal phase locking—emerging in boreal spring, growing through summer, peaking in fall, and decaying in winter.

When the ITF is blocked, the character of the ETIO cooling events changes prominently, with the occurrence of ETIO cooling events with extremely larger amplitudes (Fig. 13). The ETIO cooling in NOITF exhibits similar seasonality as that in CTRL (Fig. 14), suggesting that the stronger ETIO cooling events in NOITF have similar atmosphere–ocean coupled dynamics as in CTRL (discussed below).

Why is the amplitude of ETIO cooling events so amplified in the no-ITF scenario? To explore this question, we compare the mean states of ETIO and the composite anomalies of ETIO cooling events in the two experiments (Fig. 14). The distribution of the ETIO SST during SON in NOITF is bimodal (Fig. 14c), which renders its time average less meaningful in defining the mean of the system. Instead, we define two "modes" based on the ETIO SST during SON: the COOL state (SON ETIO SST < 26.5°C; 87 yr) and the WARM state (SON ETIO SST > 27.5°C; 67 yr) (see Fig. 14c for the marks of 26.5° and 27.5°C). We consider the WARM states in both CTRL and NOITF as the "background" state (i.e., the state upon which the ETIO cooling events occur), while the COOL state in NOITF represents the enhanced ETIO cooling state.

The composite anomalies associated with ETIO cooling events in NOITF can be approximated as the average difference between the COOL and WARM states in NOITF (Fig. 15). In boreal spring (MAM) the anomalies are weak but noticeable. The thermocline shoals in the ETIO, and SST is below normal off of Java–Sumatra. There are positive rainfall anomalies over Indonesia and the southeast tropical Indian Ocean, and negative rainfall anomalies over the central tropical Indian Ocean. Meanwhile, anomalous southeasterlies prevail south of the equator. In boreal summer (JJA), all anomaly fields grow in magnitude. By boreal fall (SON) the anomaly fields reach maximum and then decay in boreal winter (DJF). The relation among the anomalous fields in JJA and SON depict the typical atmosphere–thermocline coupled feedbacks that operate during ETIO cooling events in CTRL (see Song et al. 2007 for analysis of CTRL): cool SSTA off of Java–Sumatra causes reduced rainfall, and the anomalous diabatic heating raises local sea level pres-

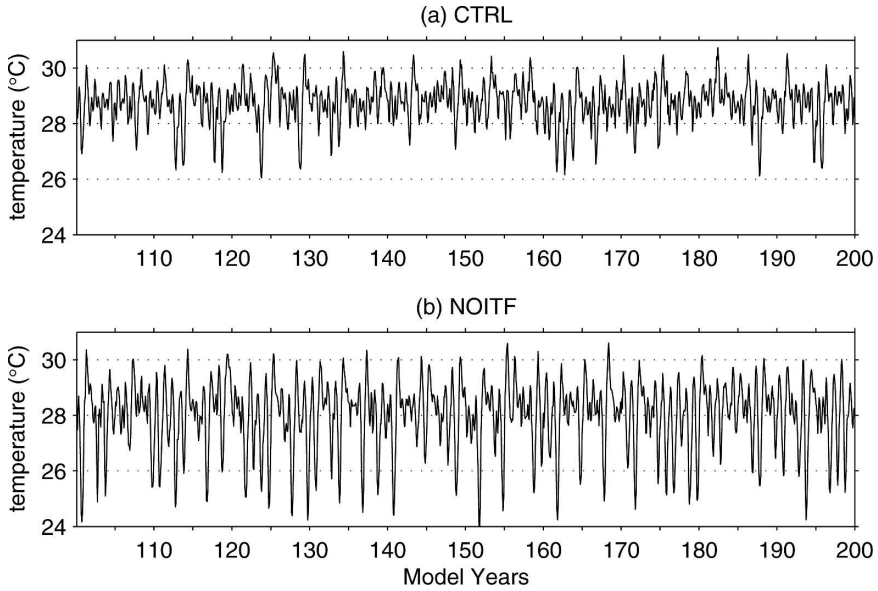

FIG. 13. Time series of the SST of the eastern tropical Indian Ocean (~10°S–0°, ~90°–110°E) in (a) CTRL and (b) NOITF runs. Only the last 100 yr are shown.

sure and drives southeasterly wind anomalies that reinforce the coastal upwelling off of Java–Sumatra and further cool the SST. Therefore, the coupled dynamics that are responsible for the ETIO cooling events in NOTIF are essentially the same as in those the CTRL run, but with much stronger intensities.

Now we contrast the WARM states in the two experiments to examine the difference in background states of ETIO. We note that there are no significant differences in SST, precipitation, and surface winds (not shown), indicating that most features of mean difference shown in Fig. 4 for those variables can be attributed to the enhanced ETIO cooling activity in NOITF. However, the difference between the ETIO thermocline depth and ocean stratification in the WARM states of the two experiments is substantial (Fig. 16). In NOITF the absence of warm ITF water results in both a shallow thermocline along the coast of Java–Sumatra, and a stronger stratification within the thermocline, which is also shown in previous OGCM studies. We suggest that the shoaled thermocline and strengthened vertical temperature gradients in ETIO are most likely responsible for the strong and frequent occurrence of ETIO cooling events in the NOITF scenario.

6. Discussion

We showed in section 5 that the mean-state difference between the ITF-on and -off scenarios (especially for SST and atmospheric variables) is, to a large extent, due to the difference in the character of the interannual variability. That raises the question of how to separate changes in the background state from changes in the

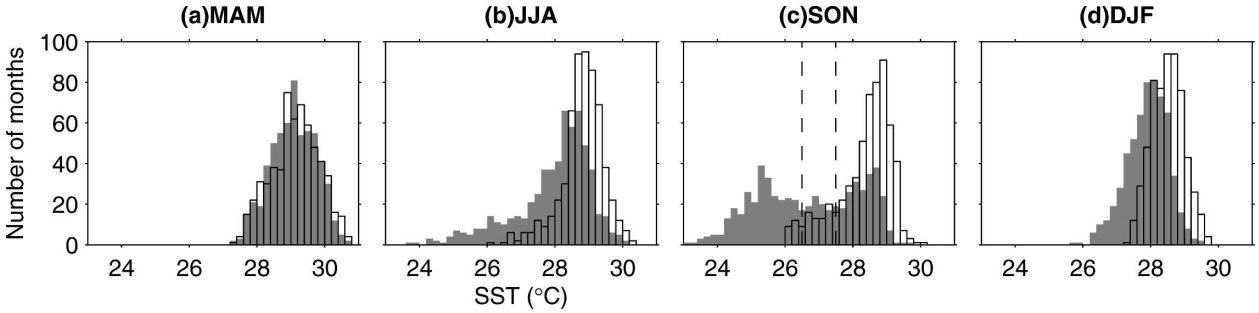

FIG. 14. Histograms of monthly SST of the eastern tropical Indian Ocean (~10°S–0°, ~90°– 110°E; first row) in four seasons. (c) The threshold temperatures (26.5° and 27.5°C) for the definition of WARM and COOL states in section 5b are indicated.

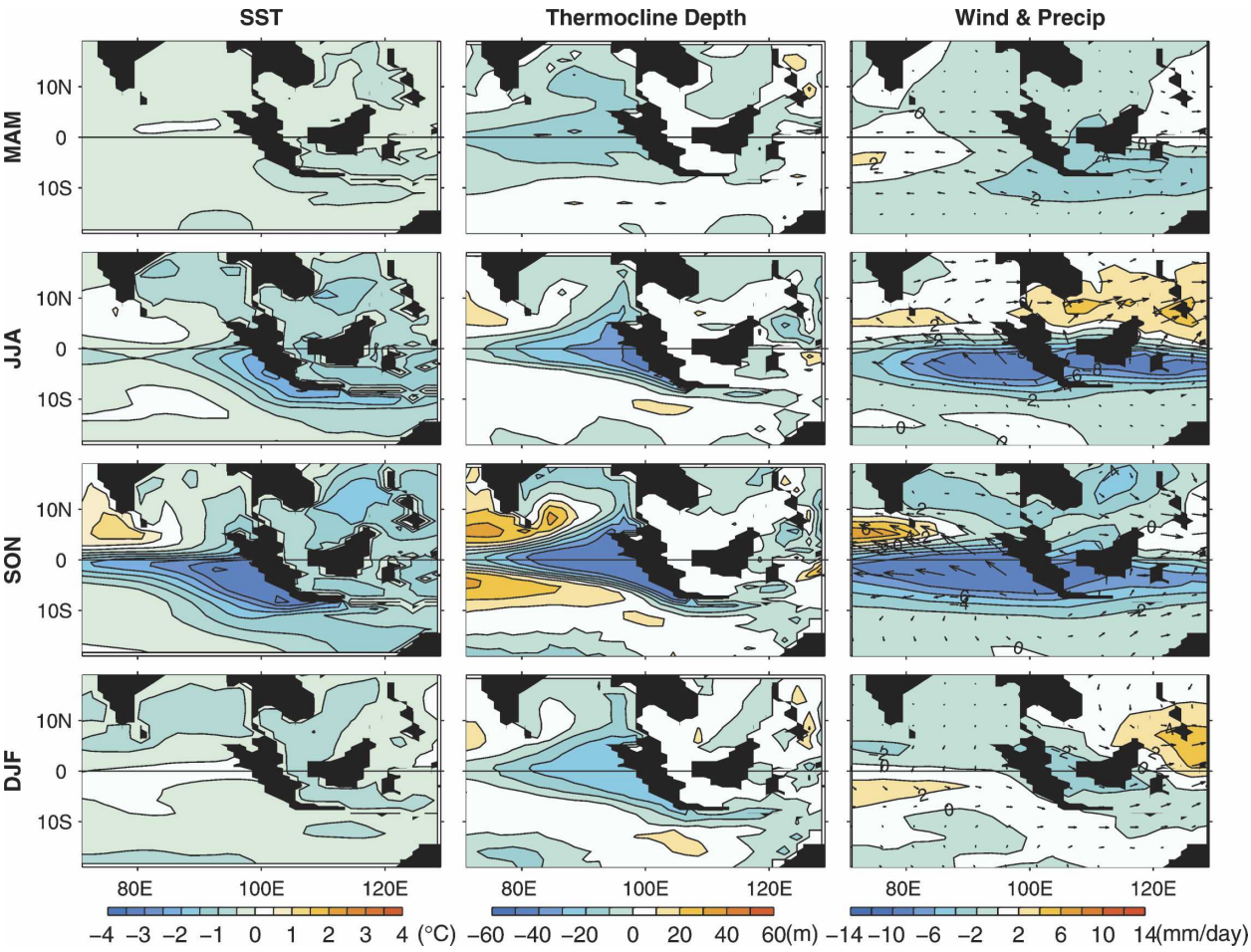

FIG. 15. Differences in SST, thermocline depth (defined as the level of maximum vertical temperature gradient), precipitation, and surface winds between COOL and WARM states in NOITF.

variability about the background. The two signals are intermingled, because the mean is generally calculated as the average over a period of time that includes anomalous events, and the anomalies associated with the variability signal are computed by extracting this mean. Clear definitions of the two signals are crucial when one contrasts mean and variability among perturbation experiments. Under such a circumstance, a common practice is to calculate mean and variability within each perturbation experiment. However, as shown in this study, the comparison of such defined means and variability among perturbation experiments may not be physically representative. We made use of the probability density distributions of climatic variables and divided the system into various states based on thresholds that distinguished "modes" in the distributions. The method turns out to be effective for the purpose of this study. We hope our results draw attention to this issue, which at first glance appears semantic but was fundamental to this analysis.

Our results provide clues for the qualitative understanding of the behavior of coupled models, and useful guidance to numerical modelers to refine their model simulation and prediction. Principally, our results suggest that a reasonable representation of ITF in climate models is necessary. We expect a coupled model with too strong (e.g., >20 Sv) or too weak (e.g., 1~2 Sv) ITF transport to produce distorted simulations of both the mean state and variability of the Tropics. We also expect the difference between models with stronger ITF and models with weaker ITF to qualitatively resemble the difference between CTRL and NOITF. However, this remains to be explored.

There are two main issues that limit the application of our results in analyzing real-world conditions. First, NOITF is highly idealized; the ITF has not been observed to shut off in the historical record. Second, by comparing open- and closed-ITF scenarios, we omit the effects of baroclinic ITF transport on tropical climate [see Song and Gordon (2004) for discussion of the im-

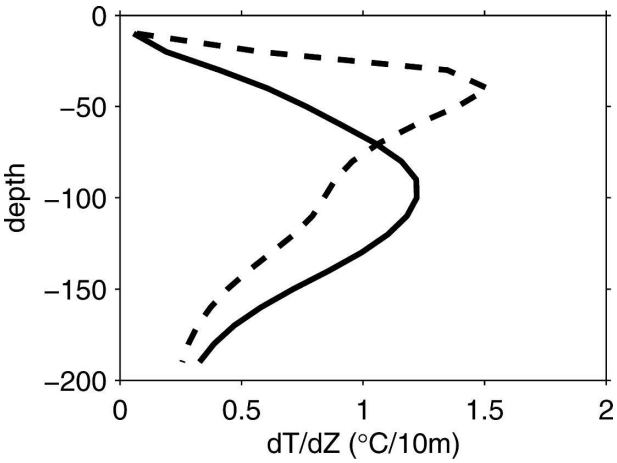

FIG. 16. Profiles of vertical temperature gradient (dT/dZ) averaged between 10°S–0°, 100°–110°E and for the WARM states of CTRL (solid line) and NOITF (dashed line).

portance of ITF baroclinic structure]. In other words, the closed-ITF situation is not equivalent to the open but zero-transport ITF situation. Because of such limitations, the results of this study are not able to give quantitative answers to questions of practical interest. The following are examples of such questions: to what extent can ITF transport variation, in particular on interannual and longer time scales, influence the variability of the Indo–Pacific domain? How accurately must coupled climate models simulate the ITF in order to reproduce and predict anomalous events (such as ENSO) and address climate change issues? For example, we notice that peak-to-trough ITF transport variation in the model is about 5–6 Sv (Fig. 2), which is about 50% of the mean ITF transport in the model (11.7 Sv). However, this does not mean that the effects resulting from such interannual ITF transport variation are 50% in magnitude of those shown in this study, because, in part, 1) the response of the tropical Indo–Pacific climate to ITF is nonlinear, 2) the change in baroclinic structure of ITF transport associated with the total ITF transport variation is unclear, and 3) the time scale for the ITF-induced changes to appear (which has been neglected in the present study) remain to be understood.

The results of this study also provide guidance in interpreting observational results. Qu et al. (1994) find that the ITF plays an important role in the surface layer heat budget of the region between Australia and Indonesia. In section 5b we show that the closure of ITF, by elevating and strengthening the thermocline, results in much stronger and more frequent occurrence of anomalous SST cooling in the ETIO, which is a key feature of the IODZM. The result therefore implies that the ITF can play a role in preconditioning the ocean conditions for the occurrence of IODZM events. The observational study of Annamalai et al. (2003) finds correlation between the interannual ITF transport and the occurrence of IODZM. Yet, more perturbation experiments are needed to quantify the physical significance of the link between the interannual ITF transport and the IODZM.

Another implication concerns the effects of ITF on ENSO characters at low frequency (such as millennial scale). It has been shown that the intensity of ENSO has undergone significant climatic shifts in the Holocene (e.g., Rodbell et al. 1999). It is still an open question as to what mechanisms are responsible for the shifts. Our results suggest that the ITF can exert significant influence on the characters of ENSO. Furthermore, recent effort in reconstructing the ITF transport in Holocene indicates that the variation of ITF transport on the millennial scale might be substantially larger than the observed interannual variability (Rosenthal et al. 2005). Therefore, we speculate that changes in the ITF may play a role in regulating the change of the character of ENSO during Holocene, and possibly other eras in the paleoclimate record.

7. Summary

In this study we employ a coupled general circulation model recently developed at the NOAA/GFDL to study the response of the Indo–Pacific tropical climate to the closure of ITF. Two experiments are performed—one with the ITF passages open and the other with them closed by land bridges in the Indonesian Seas. In the control experiment (with the ITF open) the model reasonably reproduces many aspects of the global climate, including a mean ITF transport of 11.7 Sv and its seasonal variation. In each experiment the model is integrated for 200 yr, which is a record length that allows us to explore the effects of ITF on the interannual variability of the Indo–Pacific.

The closure of ITF causes noticeable changes to the mean climate states: the strength of the South Equatorial Current and Agulhas Current in the Indian Ocean is reduced and that of the East Australian Current in the Pacific is enhanced; the upper Indian Ocean becomes cooler (thermocline is elevated); the tropical Pacific becomes warmer in the east and cooler in the west (thermocline of the equatorial Pacific is flatter); SST in the eastern equatorial Pacific becomes warmer, while that in the western equatorial Pacific becomes cooler; SST in the Indian Ocean is cooler, in particular in the eastern tropical region; and the tropical deep convection moves toward the east, which is associated with

relaxed trade winds in the tropical Pacific and anomalous easterlies in the Indian Ocean. Those mean-state changes are consistent with those from previous studies. However, we find that to a large extent the mean-state differences in SST and atmospheric fields in the Tropics are due to the changes in the character of the interannual variability in the Indo–Pacific domain, because the mean state is simply calculated as time average. In addition, it turns out that the closure of ITF induces meaningful background changes to the ocean subsurface, especially to thermocline depth and ocean stratification, which have importance in affecting atmosphere–thermocline coupling.

A major finding of this study is the effects of ITF on the interannual variability of the tropical Indo-Pacific. In the eastern tropical Indian Ocean, although the ETIO cooling events (which is a component of the so-called Indian Ocean dipole/zonal mode) have similar seasonality and atmosphere–thermocline coupled feedbacks in ITF-on and -off scenarios, they become substantially stronger when the ITF is closed. This enhancement results from enhanced atmosphere–thermocline coupling resulting from the elevated and strengthened thermocline off of Java–Sumatra. In the tropical Pacific, ENSO variability also becomes stronger and its period becomes shorter when the ITF is closed. The enhanced ENSO variability is mainly due to the occurrence of stronger warm ENSO events, because the magnitude of cool ENSO events does not significantly change. In addition, the structure of warm ENSO changes: the anomalies of SST, precipitation, and surface westerly winds are shifted to the east, and the meridional width of westerly anomalies is larger.

This study suggests that the ITF is important in regulating both the mean state and the characteristics of ENSO and Indian Ocean variability. Coupled climate models need to reasonably reproduce the ITF in order to refine their simulation and prediction of variability of the Indo–Pacific and to address issues in climate change.

Acknowledgments. This report was prepared by Dr. Qian Song under Award NA17RJ2612 from the National Oceanic and Atmospheric Administration, U.S. Department of Commerce.

REFERENCES

An, S.-I., and B. Wang, 2000: Interdecadal change of the structure of the ENSO mode and its impact on the ENSO frequency. *J. Climate,* **13,** 2044–2055.

Annamalai, H., and R. Murtugudde, 2004: Role of the Indian Ocean in regional climate variability. *Earth Climate: The Ocean–Atmosphere Interaction, Geophys. Monogr.,* Vol. 147, Amer. Geophys. Union, 213–246.

——, ——, J. Potemra, S.-P. Xie, P. Liu, and B. Wang, 2003: Coupled dynamics over the Indian Ocean: Spring initiation of the zonal mode. *Deep-Sea Res. II,* **50,** 2305–2330.

Carton, J. A., G. Chepurin, X. Cao, and B. S. Giese, 2000a: A simple ocean data assimilation analysis of the global upper ocean 1950–95. Part I: Methodology. *J. Phys. Oceanogr.,* **30,** 294–309.

——, ——, and X. Cao, 2000b: A simple ocean data assimilation analysis of the global upper ocean 1950–95. Part II: Results. *J. Phys. Oceanogr.,* **30,** 311–326.

Clarke, A. J., 1991: On the reflection and transmission of low-frequency energy at the irregular western Pacific Ocean boundary. *J. Geophys. Res.,* **96,** 3289–3305.

Delworth, T. L., and Coauthors, 2006: GFDL's CM2 global coupled climate models. Part I: Formulation and simulation characteristics. *J. Climate,* **19,** 643–674.

du Penhoat, Y., and M. A. Cane, 1991: Effect of low-latitude western boundary gaps on the reflection of equatorial motions. *J. Geophys. Res.,* **96,** 3307–3322.

England, M. H., and F. Huang, 2005: On the interannual variability of the Indonesian Throughflow and its linkage with ENSO. *J. Climate,* **18,** 1435–1444.

Fedorov, A. V., and S. G. Philander, 2000: Is El Nino changing? *Science,* **288,** 1997–2002.

Ffield, A., and A. L. Gordon, 1992: Vertical mixing in the Indonesian thermocline. *J. Phys. Oceanogr.,* **22,** 184–195.

Gent, P., and J. McWilliams, 1990: Isopycnal mixing in ocean circulation models. *J. Phys. Oceanogr.,* **20,** 150–155.

GFDL Global Atmospheric Model Development Team, 2004: The new GFDL global atmosphere and land model AM2–LM2: Evaluation with prescribed SST simulations. *J. Climate,* **17,** 4641–4673.

Gnanadesikan, A., and Coauthors, 2006: GFDL's CM2 global coupled climate models. Part II: The baseline ocean simulation. *J. Climate,* **19,** 675–697.

Godfrey, J. S., 1996: The effect of the Indonesian throughflow on ocean circulation and heat exchange with the atmosphere: A review. *J. Geophys. Res.,* **101,** 12 217–12 238.

Gordon, A. L., 1986: Interocean exchange of thermocline water. *J. Geophys. Res.,* **91,** 5037–5047.

——, 2001: Interocean exchange. *Ocean Circulation and Climate,* G. Siedler, J. Church, and J. Gould, Eds., Academic Press, 303–314.

——, 2005: Oceanography of the Indonesian Seas and their throughflow. *Oceanography,* **18,** 14–27.

——, R. D. Susanto, and A. Ffield, 1999: Throughflow within Makassar Straight. *Geophys. Res. Lett.,* **26,** 3325–3328.

Griffies, S., 1998: The Gent–McWilliams skew flux. *J. Phys. Oceanogr.,* **28,** 831–841.

Gualdi, S., E. Guilyardi, A. Navarra, S. Masina, and P. Delecluse, 2003: The interannual variability in the Indian Ocean as simulated by a CGCM. *Climate Dyn.,* **20,** 567–582.

Haney, R. L., 1971: Surface thermal boundary conditions for ocean circulation models. *J. Phys. Oceanogr.,* **1,** 241–248.

Harrison, D. E., 1987: Monthly mean island surface winds in the central tropical Pacific and El Niño. *Mon. Wea. Rev.,* **115,** 3133–3145.

——, and G. A. Vecchi, 1999: On the termination of El Niño. *Geophys. Res. Lett.,* **26,** 1593–1596.

Hirst, A. C., and J. S. Godfrey, 1993: The role of Indonesian Throughflow in a global ocean GCM. *J. Phys. Oceanogr.,* **23,** 1057–1086.

Huang, B., and J. L. Kinter III, 2002: Interannual variability in the

tropical Indian Ocean. *J. Geophys. Res.,* **107,** 3199, doi:10.1029/2001JC001278.

Hughes, T. M., A. J. Weaver, and J. S. Godfrey, 1992: Thermohaline forcing of the Indian Ocean by the Pacific Ocean. *Deep-Sea Res.,* **39,** 965–995.

Jin, F., 1997: An equatorial ocean recharge paradigm for ENSO. Part I: Conceptual model. *J. Atmos. Sci.,* **54,** 811–829.

Kleeman, R., and S. B. Power, 1995: A simple atmospheric model of surface heat flux for use in ocean modeling studies. *J. Phys. Oceanogr.,* **25,** 92–105.

Large, W. G., J. C. McWilliams, and S. C. Doney, 1994: Oceanic vertical mixing: A review and a model with a vertical K-profile boundary layer parameterization. *Rev. Geophys.,* **32,** 363–403.

Larkin, N. K., and D. E. Harrison, 2002: ENSO warm (El Niño) and cold (La Niña) event life cycles: Ocean surface anomaly patterns, their symmetries, asymmetries, and implications. *J. Climate,* **15,** 1118–1140.

Lau, N.-C., and M. J. Nath, 2003: Atmosphere–ocean variations in the Indo-Pacific sector during ENSO episodes. *J. Climate,* **16,** 3–20.

——, and ——, 2004: Coupled GCM simulation of atmosphere–ocean variability associated with zonally asymmetric SST changes in the tropical Indian Ocean. *J. Climate,* **17,** 245–265.

——, A. Leetmaa, M. J. Nath, and H. Wang, 2005: Influences of ENSO-induced Indo-western Pacific SST anomalies on extratropical atmospheric variability during the boreal summer. *J. Climate,* **18,** 2922–2942.

Lee, T., I. Fukumori, D. Menemenlis, Z. Xing, and L. Fu, 2002: Effects of the Indonesian Throughflow on the Pacific and Indian Ocean. *J. Phys. Oceanogr.,* **32,** 1404–1429.

Li, T., B. Wang, C.-P. Chang, and Y. Zhang, 2003: A theory for the Indian Ocean dipole–zonal mode. *J. Atmos. Sci.,* **60,** 2119–2135.

Lukas, R., and E. Lindstrom, 1991: The mixed layer of the Western Equatorial Pacific. *J. Geophys. Res.,* **96,** 3343–3357.

Meyers, G., 1996: Variation of Indonesian Throughflow and the El Niño-Southern Oscillation. *J. Geophys. Res.,* **101,** 12 255–12 263.

——, R. J. Bailey, and A. P. Worby, 1995: Geostrophic transport of Indonesian Throughflow. *Deep-Sea Res.,* **42,** 1163–1174.

Murtugudde, R., and A. J. Busalacchi, 1999: Interannual variability of the dynamics and thermodynamics of the tropical Indian Ocean. *J. Climate,* **12,** 2300–2326.

——, ——, and J. Beauchamp, 1998: Seasonal-to-interannual effects of the Indonesian throughflow on the tropical Indo-Pacific Basin. *J. Geophys. Res.,* **103,** 21 425–21 441.

——, J. P. McCreary, and A. J. Busalacchi, 2000: Oceanic processes associated with anomalous events in the Indian Ocean with relevance to 1997–1998. *J. Geophys. Res.,* **105,** 3295–3306.

Qu, T., G. Meyers, and J. S. Godfrey, 1994: Ocean dynamics in the region between Australia and Indonesia and its influence on the variation of sea surface temperature in a global general circulation model. *J. Geophys. Res.,* **99,** 18 433–18 445.

Rodbell, D. T., G. O. Seltzer, D. M. Anderson, M. B. Abbott, D. B. Enfield, and J. H. Newman, 1999: An ~15,000-year record of El Nino-driven alluviation in southwestern Ecuador. *Science,* **283,** 516–520.

Rosenthal, Y., D. W. Oppo, B. Linsley, Y. S. Djajadihardja, A. Ridlo, and F. Syamsudin, 2005: Reconstructing Holocene climate variability and the Indonesian Throughflow in the western equatorial Pacific. *Eos, Trans. Amer. Geophys. Union,* **86** (Fall Meeting Suppl.), Abstract OS13A-05.

Saji, N. H., S.-P. Xie, and T. Yamagata, 2006: Tropical Indian Ocean variability in the IPCC twentieth-century simulations. *J. Climate,* **19,** 4397–4417.

——, B. N. Goswami, P. N. Vinayachandran, and T. Yamagata, 1999: A dipole mode in the tropical Indian Ocean. *Nature,* **401,** 360–363.

Schneider, N., 1998: The Indonesian Throughflow and the global climate system. *J. Climate,* **11,** 676–689.

Seager, R., N. Harnik, Y. Kushnir, W. Robinson, and J. Miller, 2003: Mechanisms of hemispherically symmetric climate variability. *J. Climate,* **16,** 2960–2978.

Song, Q., and A. L. Gordon, 2004: Significance of the vertical profile of the Indonesian Throughflow to the Indian Ocean. *Geophys. Res. Lett.,* **32,** L16307, doi:10.1029/2004GL020360.

——, G. A. Vecchi, and A. J. Rosati, 2007: Indian Ocean variability in the GFDL coupled climate model. *J. Climate,* in press.

Spall, M. A., and J. Pedlosky, 2005: Reflection and transmission of equatorial Rossby waves. *J. Phys. Oceanogr.,* **35,** 363–373.

Stouffer, R., and Coauthors, 2006: GFDL's CM2 global coupled climate models. Part IV: Idealized climate response. *J. Climate,* **19,** 723–740.

Vecchi, G. A., 2006: The termination of the 1997–98 El Niño event. Part II: Mechanisms of atmospheric change. *J. Climate,* **19,** 2647–2664.

——, and D. E. Harrison, 2003: On the termination of the 2002–03 El Niño event. *Geophys. Res. Lett.,* **30,** 1964, doi:10.1029/2003GL017564.

——, and D. E. Harrison, 2006: The termination of the 1997–98 El Niño event. Part I: Mechanisms of oceanic change. *J. Climate,* **19,** 2633–2646.

——, A. T. Wittenberg, and A. Rosati, 2006: Reassessing the role of stochastic forcing in the 1997–1998 El Niño. *Geophys. Res. Lett.,* **33,** L01706, doi:10.1029/2005GL024738.

Vranes, K., A. L. Gordon, and A. Ffield, 2002: The heat transport of the Indonesian throughflow and implications for the Indian Ocean heat budget. *Deep-Sea Res. II,* **49,** 1391–1410.

Wajsowicz, R. C., 2004: Climate variability over the tropical Indian Ocean sector in the NSIPP seasonal forecast system. *J. Climate,* **17,** 4783–4804.

——, and E. K. Schneider, 2001: The Indonesian Throughflow's effect on global climate determined from the COLA Coupled Climate System. *J. Climate,* **14,** 3029–3042.

Webster, P. J., A. M. Moore, J. P. Loschnigg, and R. R. Leben, 1999: Coupled ocean-atmosphere dynamics in the Indian Ocean during 1997–98. *Nature,* **401,** 356–360.

Wittenberg, A. T., 2002: ENSO response to altered climates. Ph.D. thesis, Princeton University, 475 pp.

——, 2004: Extended wind stress analyses for ENSO. *J. Climate,* **17,** 2526–2540.

——, A. Rosati, N.-C. Lau, and J. J. Ploshay, 2006: GFDL's CM2 global coupled climate models. Part III: Tropical Pacific climate and ENSO. *J. Climate,* **19,** 698–722.

Wyrtki, K., 1973: An equatorial jet in the Indian Ocean. *Science,* **181,** 262–264.

Yamagata, T., S. K. Behera, J.-J. Luo, S. Masson, M. R. Jury, and S. A. Rao, 2004: Coupled ocean–atmosphere variability in the tropical Indian Ocean. *Earth Climate: The Ocean–Atmosphere Interaction, Geophys. Monogr.,* Vol. 147, Amer. Geophys. Union, 189–211.